




## ARTICLE

Heme oxygenase-1 inhibition promotes IFN $\gamma$ - and NOS2-mediated control of *Mycobacterium tuberculosis* infection

Diego L. Costa<sup>1</sup> , Eduardo P. Amaral<sup>1</sup>, Sivaranjani Namasivayam<sup>1</sup>, Lara R. Mittereder<sup>1</sup>, Logan Fisher<sup>1</sup>, Caio C. Bonfim<sup>1</sup>, Aline Sardinha-Silva<sup>2</sup>, Robert W. Thompson<sup>3</sup>, Sara E. Hieny<sup>1</sup>, Bruno B. Andrade<sup>1,4,5,6,7,8,9,10</sup> and Alan Sher<sup>1</sup>

*Mycobacterium tuberculosis* (Mtb) infection induces pulmonary expression of the heme-degrading enzyme heme oxygenase-1 (HO-1). We have previously shown that pharmacological inhibition of HO-1 activity in experimental tuberculosis results in decreased bacterial loads and unexpectedly that this outcome depends on the presence of T lymphocytes. Here, we extend these findings by demonstrating that IFN $\gamma$  production by T lymphocytes and NOS2 expression underlie this T-cell requirement and that HO-1 inhibition potentiates IFN $\gamma$ -induced NOS2-dependent control of Mtb by macrophages in vitro. Among the products of heme degradation by HO-1 (biliverdin, carbon monoxide, and iron), only iron supplementation reverted the HO-1 inhibition-induced enhancement of bacterial control and this reversal was associated with decreased NOS2 expression and NO production. In addition, we found that HO-1 inhibition results in decreased labile iron levels in Mtb-infected macrophages in vitro and diminished iron accumulation in Mtb-infected lungs in vivo. Together these results suggest that the T-lymphocyte dependence of the therapeutic outcome of HO-1 inhibition on Mtb infection reflects the role of the enzyme in generating iron that suppresses T-cell-mediated IFN $\gamma$ /NOS2-dependent bacterial control. In broader terms, our findings highlight the importance of the crosstalk between iron metabolism and adaptive immunity in determining the outcome of infection.

*Mucosal Immunology* \_\_\_\_\_; <https://doi.org/10.1038/s41385-020-00342-x>

## INTRODUCTION

Tuberculosis (TB), resulting from infection with the bacterium *Mycobacterium tuberculosis* (Mtb), is now the leading cause of mortality due to a single infectious agent.<sup>1</sup> Although antibiotic therapy for Mtb has been available for almost 80 years,<sup>2</sup> its effects on the global burden of TB have not kept pace with the results of interventions in the other major infectious diseases of mankind. The current treatment regimen for TB consists of four different antibiotics that typically are administered for 6–9 months and can be associated with adverse side effects. This scenario promotes noncompliance leading to both relapse and the development of drug resistance.<sup>3</sup> Indeed, multidrug resistance in TB infection is on the rise with over 390,000 cases reported in 2018.<sup>1</sup> Thus, there is a need for more effective therapeutic approaches for TB treatment and in particular, those that can promote more rapid cure and act against drug resistant organisms.

In addition to the development of more efficient antibiotics, a second approach to achieving more rapid and effective cure is to target the Mtb–host interaction with host-directed therapies (HDTs), which could be used as an adjunct to conventional drug treatment. By their nature, such therapeutic approaches do not

target the pathogen directly, thereby circumventing the development of drug resistance. A number of different strategies involving different host targets affecting Mtb susceptibility have been proposed and several are currently being tested in clinical trials.<sup>4</sup>

In a previous study, we described a novel HDT candidate based on the inhibition of heme oxygenase-1 (HO-1), a host enzyme critical for the recycling of iron,<sup>5</sup> a metal important both as essential nutrient for Mtb growth as well as for many host-defense functions.<sup>6,7</sup> We showed that the treatment of Mtb-infected mice with a well-characterized inhibitor of HO-1 enzymatic activity, tin protoporphyrin IX (SnPP), results in a reduction in pulmonary bacterial loads and when administered adjunctively with antibiotics, accelerates pathogen clearance. An unusual property of this experimental HDT is that its efficacy depends on the adaptive immune system. Thus, SnPP fails to reduce bacterial loads when administered earlier than 3 weeks post infection (wpi), before the emergence of antigen-responsive T cells, or when given to mice lacking a T-cell compartment.<sup>8</sup>

The development of a Th1 immune response is critical for the control of Mtb infection and this effect is generally attributed to the production of IFN $\gamma$  and TNF, and in murine infection, the

<sup>1</sup>Immunobiology Section, Laboratory of Parasitic Diseases, National Institute of Allergy and Infectious Diseases, National Institutes of Health, Bethesda, MD, USA; <sup>2</sup>Molecular Parasitology Section, Laboratory of Parasitic Diseases, National Institute of Allergy and Infectious Diseases, National Institutes of Health, Bethesda, MD, USA; <sup>3</sup>Helminth Immunology Section, Laboratory of Parasitic Diseases, National Institute of Allergy and Infectious Diseases, National Institutes of Health, Bethesda, MD, USA; <sup>4</sup>Wellcome Centre for Infectious Disease Research in Africa, Institute of Infectious Disease and Molecular Medicine, University of Cape Town, Observatory, Cape Town 7925, South Africa; <sup>5</sup>Instituto Gonçalo Moniz, Fundação Oswaldo Cruz, Salvador, Brazil; <sup>6</sup>Multinational Organization Network Sponsoring Translational and Epidemiological Research (MONSTER) Initiative, Salvador, Brazil; <sup>7</sup>Curso de Medicina, Faculdade de Tecnologia e Ciências (FTC), Salvador, Brazil; <sup>8</sup>Universidade Salvador (UNIFACS), Laureate Universities, Salvador, Brazil; <sup>9</sup>Escola Bahiana de Medicina e Saúde Pública (EBMSP), Salvador, Brazil and <sup>10</sup>Division of Infectious Diseases, Department of Medicine, School of Medicine, Vanderbilt University, Nashville, TN, USA

Correspondence: Diego L. Costa (dlcosta@usp.br)

Received: 31 March 2020 Revised: 17 July 2020 Accepted: 12 August 2020

Published online: 29 August 2020



induction of nitric oxide by this subset of T lymphocytes.<sup>9</sup> While IFN $\gamma$  itself has been tested clinically with mixed results as a treatment for multidrug resistant Mtb,<sup>10</sup> few if any of the other published HDT approaches directly target the Th1 response or its products. Nevertheless, in several cases candidate HDTs have been reported to enhance Th1 responses as an indirect outcome.<sup>4</sup>

In the present study, we have examined the mechanisms underlying the unusual T-cell dependence of the therapeutic effect of SnPP-mediated HO-1 inhibition on experimental Mtb infection. We present evidence that SnPP treatment results in increased NOS2 expression and NO production, thereby enhancing IFN $\gamma$ -mediated control of bacterial replication and implicate the inhibition of iron generation as the mechanism underlying this outcome. These findings suggest that in addition to affecting the availability of the metal as a nutrient for Mtb growth,<sup>11</sup> the regulation of iron metabolism can influence microbicidal mechanisms induced by IFN $\gamma$  activation in macrophages infected with the pathogen. In addition, they further support the process of iron homeostasis in Mtb-infected cells as an important target for the development of HDTs against TB.

## RESULTS

### Characterization of HO-1 expressing cells in Mtb-infected mouse lungs

We have previously demonstrated that the pharmacological inhibition of host HO-1 activity in Mtb-infected mice with tin protoporphyrin IX (SnPP) results in a highly significant and reproducible reduction in pulmonary bacterial loads and that this outcome is dependent on the presence of an intact T-cell compartment.<sup>8</sup> As a first step in studying the role of T-cell immunity in the beneficial effects of HO-1 inhibition during experimental TB, we characterized the cellular source of HO-1 expression in the lungs of infected mice. Previous studies involving immunohistochemical staining had localized HO-1 to CD68<sup>+</sup> myeloid cells in pulmonary human granulomas.<sup>12</sup> We performed flow cytometry and western blotting to further characterize the myeloid cell populations involved in our mouse model.

In agreement with our previous findings employing real-time PCR and western blotting measurement of the enzyme,<sup>8</sup> we observed a sharp increase in the expression of HO-1 in lung homogenates by ELISA beginning at 4 wpi (Fig. 1a). In order to differentiate HO-1-producing cells that are present in the circulation from those in the lung parenchyma and alveoli, we performed intravenous pan-leukocyte staining prior to euthanasia as previously described.<sup>13</sup> We distinguished the different subsets based on their expression of specific surface markers as detailed in Fig. S1a–c.

We found that alveolar macrophages express high levels of HO-1 even when obtained from naive mice and that Mtb infection results in a small but significant decrease in the frequency of HO-1<sup>+</sup> alveolar macrophages at 4 wpi (Fig. 1b, c). The frequency of HO-1<sup>+</sup> IV<sup>-</sup> neutrophils underwent an increase at 2 wpi, this elevation returned to naive levels by 4 wpi, while a small but significant increase of HO-1<sup>+</sup> neutrophils occurred in the IV<sup>+</sup> compartment at 4 wpi (Fig. 1b, c). In the remaining mononuclear myeloid cells, there was a reduction in the frequency of HO-1<sup>+</sup> cells in the IV<sup>+</sup> compartment, while the IV<sup>-</sup> mononuclear fraction displayed an enhanced frequency of HO-1<sup>+</sup> cells following Mtb infection with a major increase occurring at 4 wpi (Fig. 1b, c).

Using an mCherry-expressing Mtb strain, we identified that at 4 wpi, a time point in which we found elevated HO-1 expression in lung homogenates (Fig. 1a), Mtb-infected cells are located predominantly in the IV<sup>-</sup> compartment, suggesting that they are either in the parenchyma or alveoli (Fig. 2a). We therefore, further analyzed the IV<sup>-</sup> myeloid cells and confirmed that alveolar macrophages are the major source of the low levels of HO-1 in the

lungs of naive and 2-week-infected mice, while mononuclear myeloid cells predominate at 4 wpi (Fig. 2b) indicating that they are the principal source of the HO-1 in the lung parenchymal and alveolar compartments at that time point. Additional characterization of the HO-1<sup>+</sup> IV<sup>-</sup> mononuclear myeloid cells at 4 wpi revealed that more than 95% have a macrophage (CD11b<sup>+</sup>CD64<sup>+</sup>) phenotype, while around 70% are Ly6C<sup>+</sup>, indicating that the majority are of inflammatory monocyte origin (Fig. 2c). We then sorted the parenchymal and alveolar myeloid cells from Mtb-infected mouse lungs at 4 wpi, and further separated the CD11b<sup>+</sup> mononuclear myeloid cells into Ly6C<sup>-</sup> and Ly6C<sup>+</sup> subsets in order to compare their HO-1 production by western blot. The results confirmed the flow cytometry analysis demonstrating that CD11b<sup>+</sup>Ly6C<sup>+</sup> cells are the major HO-1 expressing myeloid cell population (Fig. 2d).

We next performed experiments in which mice were infected with an mCherry-expressing Mtb strain in order to determine whether HO-1 expression is limited to infected cells. When assayed 4 weeks later, we found that within the entire parenchymal and alveolar myeloid cell population there is a large proportion of HO-1<sup>+</sup> cells that are uninfected. This was particularly true for alveolar macrophages where only around 2% of the HO-1<sup>+</sup> cells are Mtb-infected (Fig. 2e). In contrast, in neutrophils as well as CD11b<sup>+</sup>Ly6C<sup>-</sup> and CD11b<sup>+</sup>Ly6C<sup>+</sup> mononuclear myeloid cells, a larger frequency of HO-1<sup>+</sup> cells are Mtb infected (20.1%, 23.2%, and 22.4% respectively) (Fig. 2e). However, when we analyzed HO-1 expression only in Mtb-infected cells within the IV<sup>-</sup> parenchymal/alveolar compartment, we found that the overwhelming majority of Mtb<sup>+</sup> alveolar macrophages, Ly6C<sup>+</sup> and Ly6C<sup>-</sup> CD11b<sup>+</sup> mononuclear myeloid cells are positive for HO-1 (91.3%, 95.1%, and 95.8% respectively), whereas only 26.2% of Mtb<sup>+</sup> neutrophils express the enzyme (Fig. 2f). Together these results confirmed that mononuclear myeloid cells are the main source of HO-1 in the pulmonary parenchyma and alveoli of Mtb-acutely infected mice and that virtually all of these cells if infected with the bacillus express HO-1 (Fig. 2g).

### IFN $\gamma$ production by T cells is required for bacterial load reduction upon HO-1 pharmacological inhibition

HO-1 inhibition during murine TB is only effective in reducing pulmonary bacterial loads when treatment with tin protoporphyrin (SnPP) is initiated after the third week of infection, a time point at which expression of the enzyme is first detected in lung homogenates.<sup>8</sup> Compared to SnPP, treatment with cobalt protoporphyrin, a well-characterized pharmacological HO-1 inducer results in a small, nonsignificant increase in pulmonary bacterial loads (Fig. S2a), suggesting that, although the inhibition of enzyme activity favors the control of bacterial replication, a further enhancement in HO-1 expression beyond that induced by Mtb infection itself does not result in enhanced susceptibility.

The time point at which HO-1 is first detected in whole Mtb-infected mouse lungs correlates kinetically with the development of the host Th1 response to Mtb as assessed by IFN $\gamma$  and NOS2 mRNA expression and CD44<sup>+</sup>Tbet<sup>+</sup> CD4<sup>+</sup> T-cell expansion in the lungs (Fig. S2b–d) as well as with the expression of HO-1 in the parenchymal and alveolar mononuclear myeloid cell compartments (Fig. 1). This association suggested that the ability to respond to SnPP treatment might depend on presence of Th1 products and in particular IFN $\gamma$ . To test the latter hypothesis, C57BL/6 and IFN $\gamma$ <sup>-/-</sup> mice were infected with Mtb and treated or not with SnPP for 15 days starting at 4 wpi. While treatment with the inhibitor resulted in a significant reduction in pulmonary bacterial loads in IFN $\gamma$  sufficient C57BL/6 mice, no effect was observed in IFN $\gamma$ <sup>-/-</sup> mice (Fig. 3a). To address the source of the required IFN $\gamma$ , a similar SnPP treatment experiment was performed in T-cell deficient TCR $\alpha$ <sup>-/-</sup> mice that were adoptively transferred with total T cells from C57BL/6 or IFN $\gamma$ <sup>-/-</sup> mice 1 week prior to infection. HO-1 pharmacological inhibition resulted in

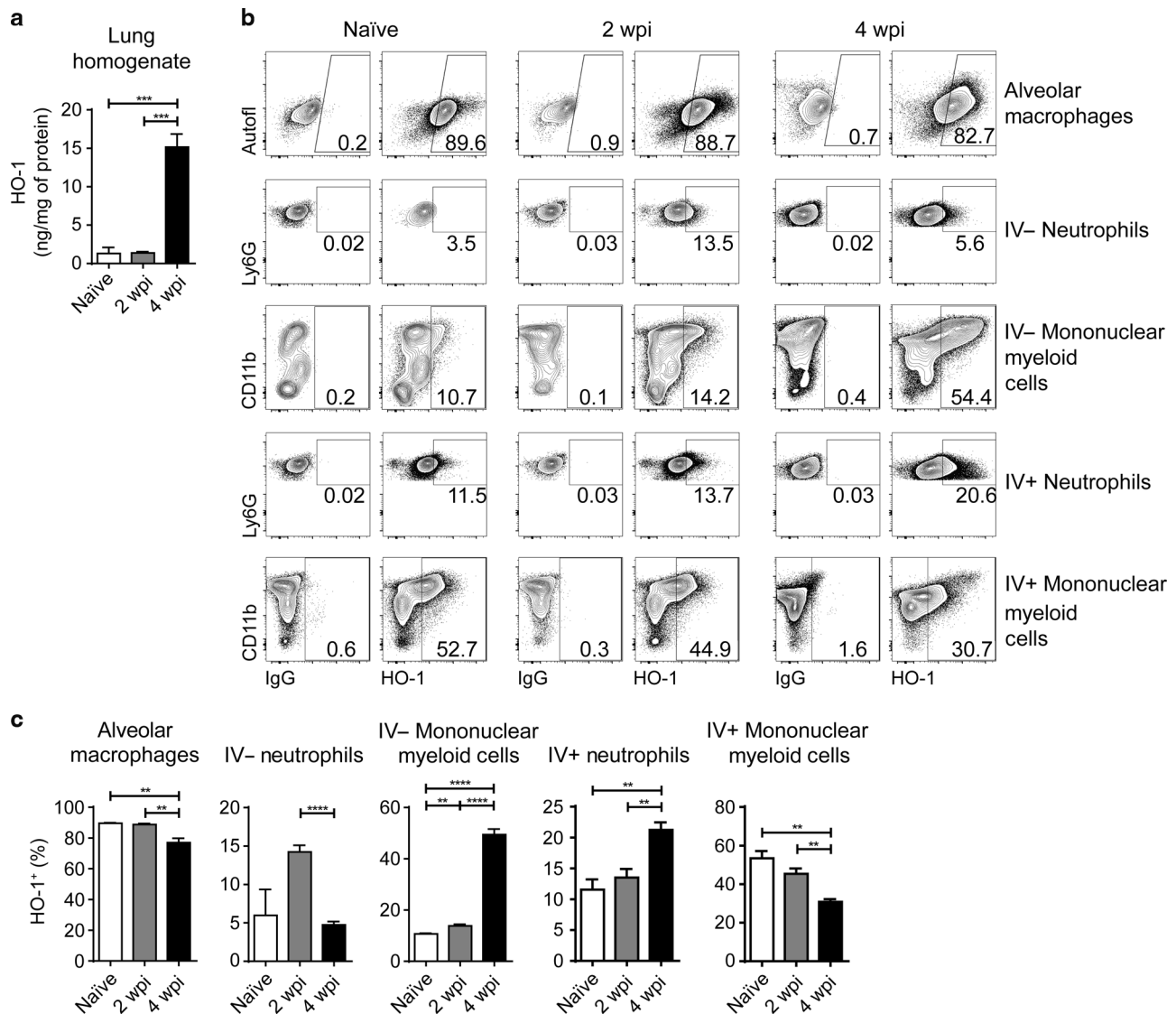


**Fig. 1** HO-1 is upregulated mainly in parenchymal and alveolar mononuclear myeloid cells in the lungs of *M. tuberculosis*-infected mice. **a** HO-1 concentration measured by ELISA in lung homogenates obtained from naive, or *M. tuberculosis*-infected mice at 2 and 4 weeks post infection (wpi) ( $n = 4$  mice/group). **b** Representative dot plots showing HO-1 staining in the right-hand columns and correspondent negative control on the left-hand columns in alveolar macrophages, parenchymal/alveolar (IV<sup>-</sup>) neutrophils and mononuclear myeloid cells as well as intravascular (IV<sup>+</sup>) neutrophils, and mononuclear myeloid cells, from lungs of naive or *M. tuberculosis*-infected mice at 2 and 4 wpi, gated as detailed in Fig. S1 (flow cytometry data concatenated from four samples). **c** Frequencies of HO-1<sup>+</sup> alveolar macrophages, parenchymal/alveolar (IV<sup>-</sup>) neutrophils, and mononuclear myeloid cells as well as intravascular (IV<sup>+</sup>) neutrophils, and mononuclear myeloid cells, measured by flow cytometry in lungs of naive or *M. tuberculosis*-infected mice at 2 and 4 wpi, gated as detailed in Fig. S1. Data shown are representative of three independent experiments. Statistical analysis: unpaired Student's t test. \*\**p* < 0.01, \*\*\**p* < 0.001, \*\*\*\**p* < 0.0001.

significant reductions in lung bacterial loads in mice adoptively transferred with C57BL/6 T cells, but not in animals receiving IFN $\gamma$ <sup>-/-</sup> T cells (Fig. 3b), arguing that the production of IFN $\gamma$  by T cells is essential for the antibacterial effects of SnPP treatment.

IFN $\gamma$  and HO-1 expression are unlinked in Mtb-infected mice The IFN $\gamma$ -dependence of SnPP therapy could reflect a role for the enzyme in downregulating Th1 development and/or IFN $\gamma$  production thereby suppressing host control of infection. This hypothesis would be consistent with previous data demonstrating a role for HO-1 in suppressing pro-inflammatory Th1 immune responses in experimental colitis and sickle cell alloimmunization.<sup>14,15</sup> Conversely, the IFN $\gamma$  requirement could simply reflect a role for the cytokine in regulating HO-1 expression in Mtb-infected myeloid cells. In order to test the first hypothesis, C57BL/6 mice were treated or not with SnPP as described previously and

pulmonary T-cell responses assessed. No difference was found in the frequency and total numbers of CD4<sup>+</sup> and CD8<sup>+</sup> T lymphocytes or in the expression of the activation marker CD44 in parenchymal/alveolar compartments of lungs from SnPP-treated versus nontreated mice (Fig. 3a-c). Moreover, the ex vivo production of IFN $\gamma$  by pulmonary parenchymal/alveolar CD4<sup>+</sup> T lymphocytes after Mtb antigen stimulation was indistinguishable between SnPP-treated and nontreated mice (Fig. S3D, E), arguing that the effect of SnPP treatment on bacterial loads is not due to HO-1-mediated downmodulation of Th1 adaptative immune responses during Mtb infection. We did however observe a small but significant increase in the frequency and number of alveolar macrophages and a more pronounced decrease in the number of parenchymal/alveolar mononuclear myeloid cells in SnPP-treated Mtb-infected mice compared to nontreated animals (Fig. S3f), which could potentially contribute

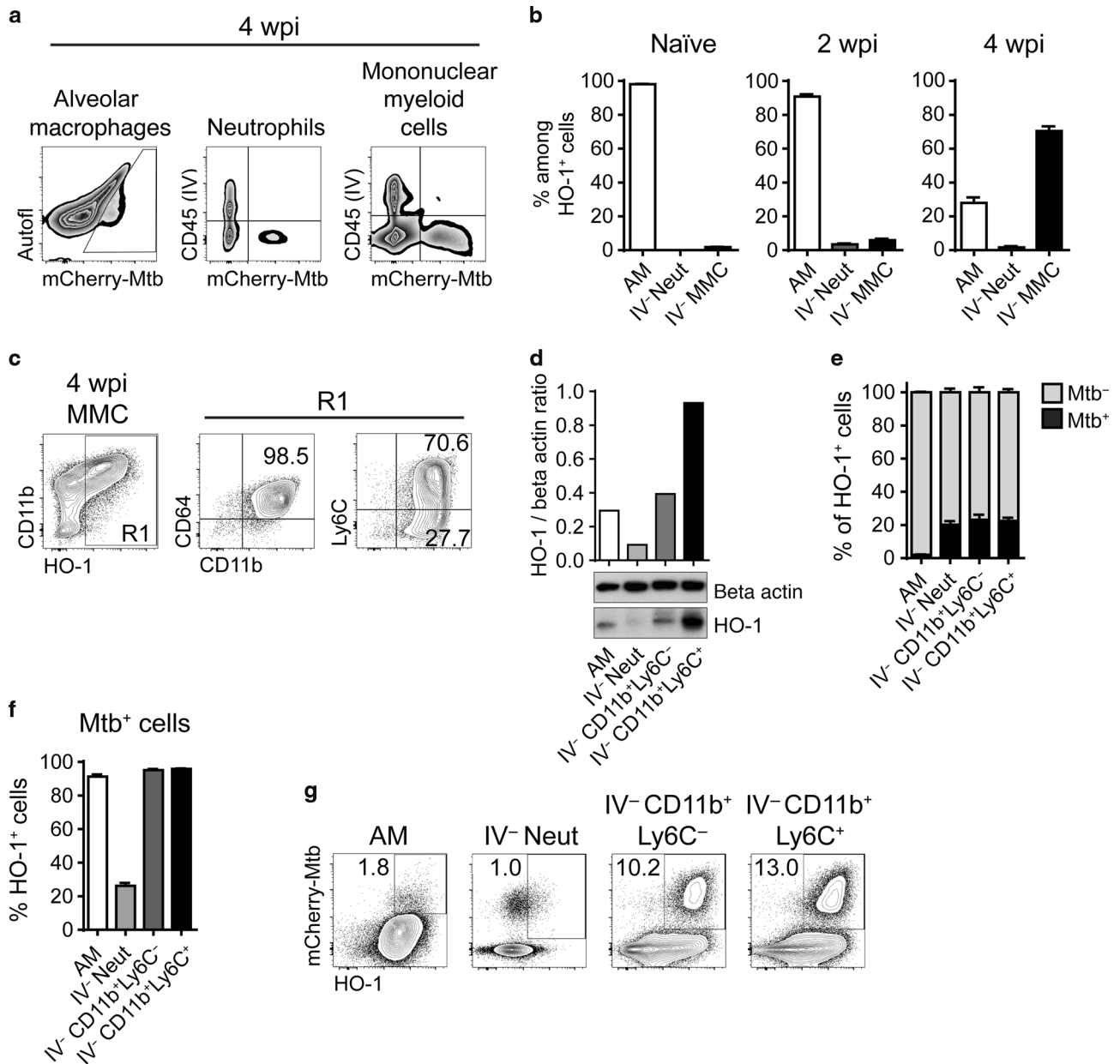
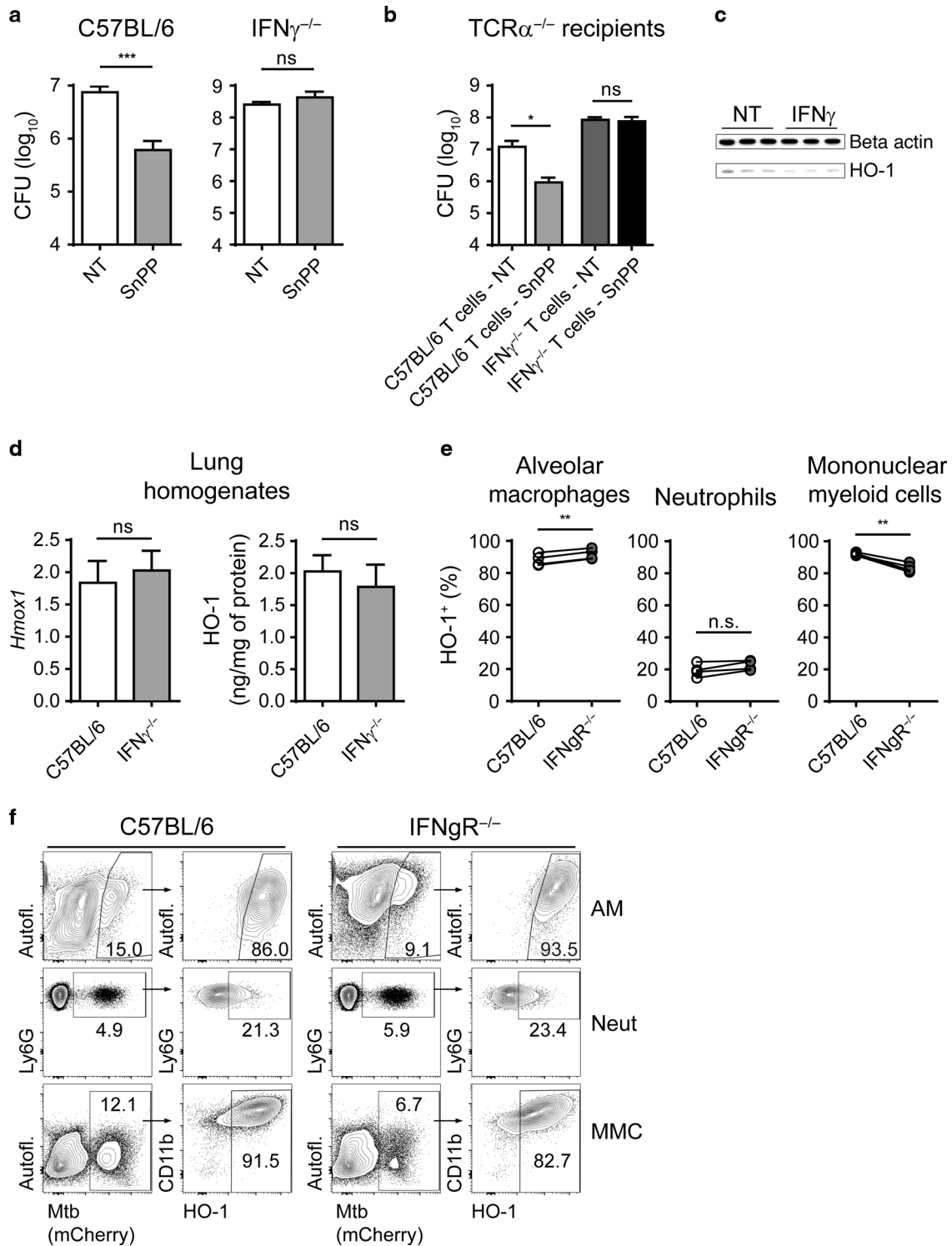


**Fig. 2 The vast majority of Mtb-infected pulmonary parenchymal and alveolar mononuclear myeloid cells express HO-1.** **a** Representative dot plots showing mCherry *M. tuberculosis* staining in alveolar macrophages and parenchymal/alveolar (CD45<sup>IV-</sup>) and intravascular (CD45<sup>IV+</sup>) neutrophils (Neut) and mononuclear myeloid cells (MMC) from lungs of *M. tuberculosis*-infected mice at 4 weeks post infection (wpi), gated as detailed in Fig. S1 (flow cytometry data concatenated from four samples). **b** Percentage represented by each cell population among parenchymal/alveolar (IV<sup>-</sup>) HO-1<sup>+</sup> cells isolated from naive, or *M. tuberculosis*-infected mice at 2 and 4 wpi ( $n = 4$  mice/group). **c** Representative dot plot showing phenotypic characterization by flow cytometry of parenchymal/alveolar (IV<sup>-</sup>) HO-1<sup>+</sup> MMC (gate R1) isolated from lungs of mice at 4 wpi with *M. tuberculosis* (flow cytometry data concatenated from four samples). **d** HO-1 and beta actin detection by western blotting (bottom) in parenchymal/alveolar (IV<sup>-</sup>) cells sorted from lungs of mice at 4 wpi according to phenotypic characteristics detailed in Fig. S1 and Fig. 2c and quantification of HO-1 in each cell population normalized to beta actin (endogenous control) expression on the same samples (top) ( $n = 4$  mice/group—pooled samples). **e** Percentage represented by Mtb-infected (black) or uninfected (gray) cells among HO-1<sup>+</sup> AM and parenchymal/alveolar (IV<sup>-</sup>) Neut, CD11b<sup>+</sup>Ly6C<sup>-</sup>, and CD11b<sup>+</sup>Ly6C<sup>+</sup> MMC ( $n = 4$  mice/group). **f** Frequency of HO-1<sup>+</sup> cells among Mtb-infected AM and parenchymal/alveolar (IV<sup>-</sup>) Neut, CD11b<sup>+</sup>Ly6C<sup>-</sup>, and CD11b<sup>+</sup>Ly6C<sup>+</sup> MMC ( $n = 4$  mice/group). **g** Representative dot plots showing HO-1 mCherry Mtb and HO-1 staining in total AM and parenchymal/alveolar (IV<sup>-</sup>) Neut, CD11b<sup>+</sup>Ly6C<sup>-</sup>, and CD11b<sup>+</sup>Ly6C<sup>+</sup> MMC populations (flow cytometry data concatenated from four samples). Data expressed as mean  $\pm$  standard error of mean (**b**, **e**, and **f**), dot plots from concatenated data (**a**, **c**, and **g**), or pooled samples (**d**). Data shown are representative of two (**a**, **e**, **f**, and **g**) or three independent experiments (**b**, **c**, and **d**).

to or be an outcome of the reduced bacterial loads observed in these animals.

In order to test the second hypothesis of a possible role for IFN $\gamma$  signaling in the induction of HO-1 expression, bone marrow derived macrophages (BMDM) were infected with Mtb and treated or not with recombinant murine IFN $\gamma$ . HO-1 expression

by Mtb-infected macrophages was only minimally affected by IFN $\gamma$  treatment (Fig. 3c). Moreover, no difference was found in the expression of either HO-1 mRNA or protein in lung homogenates of C57BL/6 and IFN $\gamma$ <sup>-/-</sup> mice at 4 wpi (Fig. 3d). However, as described above, HO-1 is expressed differentially by the different pulmonary myeloid cell subsets, which also are not equally



infected with Mtb (Fig. 2). We therefore assessed by flow cytometry if IFN $\gamma$  signaling modulates HO-1 expression in isolated Mtb-infected parenchymal and alveolar pulmonary myeloid cell populations.

In contrast with wild-type (WT) C57BL/6 animals, IFN $\gamma$ <sup>-/-</sup> mice develop an inflammatory infiltrate in the parenchyma and alveoli dominated by neutrophils (Fig. S4a, c), which also represent the most highly infected cells in the lungs of these animals (Fig. S4b, c). This major effect on neutrophil levels introduces a potential complication when comparing HO-1<sup>+</sup> cells between the two

mouse strains. We therefore employed a mixed bone marrow chimera approach in which CD45.1/2 WT mice were irradiated and reconstituted simultaneously with equal numbers of CD45.1 WT and CD45.2 IFN $\gamma$ R<sup>-/-</sup> bone marrow cells. The Mtb-infected chimeric mice had similar levels of WT and IFN $\gamma$ R<sup>-/-</sup> cells (Fig. S4d) in the lungs and in particular neutrophils and mononuclear myeloid cells in the parenchymal/alveolar compartment (Fig. S4e, g), the latter representing the major Mtb-infected subset in both WT and IFN $\gamma$ R<sup>-/-</sup> cells (Fig. S4e, f), thus justifying the validity of the chimera approach.

**Fig. 3** IFN $\gamma$  production by T cells is required for bacterial load reduction mediated by pharmacological HO-1 inhibition. **a** CFU loads in lung homogenates of C57BL/6 or IFN $\gamma$ <sup>-/-</sup> Mtb-infected mice treated or not for 15 days with SnPP ( $n = 3$  and  $4$  mice/group). **b** CFU loads in lung homogenates of TCR $\alpha$ <sup>-/-</sup> recipient mice treated or not with SnPP for 15 days (TCR $\alpha$ <sup>-/-</sup> recipient mice were adoptively transferred intravenously with  $1 \times 10^6$  total T lymphocytes isolated from spleens of naive C57BL/6 or IFN $\gamma$ <sup>-/-</sup> mice 7 days prior to infection with Mtb) ( $n = 4$  mice/group). **c** HO-1 and beta actin detection by western blot in cell lysates of BMDM cultures 24 h post infection and stimulation or not with recombinant murine IFN $\gamma$  (100 U/mL). **d** mRNA quantification by real-time PCR (left) and protein quantification by ELISA (right) of HO-1 in lung homogenates obtained from C57BL/6 and IFN $\gamma$ <sup>-/-</sup> mice at 4 weeks post infection (wpi) with Mtb ( $n = 4$  mice/group). **e** HO-1 expression measured by flow cytometry in mCherry Mtb<sup>+</sup> donor alveolar macrophages (AM), parenchymal neutrophils (Neut), or parenchymal myeloid mononuclear cells (MMC) recovered from the lungs of infected receptor mice at 4 wpi and gated as detailed in Fig. S1 (C57BL/6J  $\times$  B6.SJL F1 (CD45.1/2) mice were lethally irradiated ( $2 \times 500$  rad—4 h prior to cell transfer), injected with  $1 \times 10^7$  total bone marrow cells containing equal amounts of cells from B6/SJL (CD45.1) and IFN $\gamma$ R<sup>-/-</sup> (CD45.2) mice, and allotted 10 weeks for immune reconstitution prior to infection) ( $n = 4$  mice/group). **f** Representative dot plots from data depicted in Fig. 3e, showing gating of Mtb<sup>+</sup> cells in left-hand panels and HO-1 expression in gated cells in right-hand panels (flow cytometry data concatenated from four samples). Data expressed as mean  $\pm$  standard error of mean (**a**, **b**, and **d**), as individual samples (**c**), paired individual samples (**e**), or dot plots from concatenated data (**f**). Data shown are representative of two (**b**, **c**, and **e**) or three independent experiments (**a** and **d**). Statistical analysis: unpaired (**a**, **b**, and **d**) and paired (**e**) Student's *t* test. \* $p < 0.05$ , \*\* $p < 0.01$ , \*\*\* $p < 0.001$ , n.s. nonsignificant.

When we compared HO-1 expression in WT and IFN $\gamma$ R<sup>-/-</sup> Mtb-infected parenchymal and alveolar pulmonary myeloid cells at 4 wpi, we found a slight increase in the frequency of HO-1<sup>+</sup> alveolar macrophages in IFN $\gamma$ R<sup>-/-</sup> cells, similar frequencies of HO-1<sup>+</sup> neutrophils and a small (less than 10%) but significant reduction in HO-1 expression in IFN $\gamma$ R<sup>-/-</sup> mononuclear myeloid cells (Fig. 3e, f). Therefore, the lack of response to SnPP in the absence of IFN $\gamma$  cannot be accounted for by a wholesale impairment of HO-1 expression in infected cells.

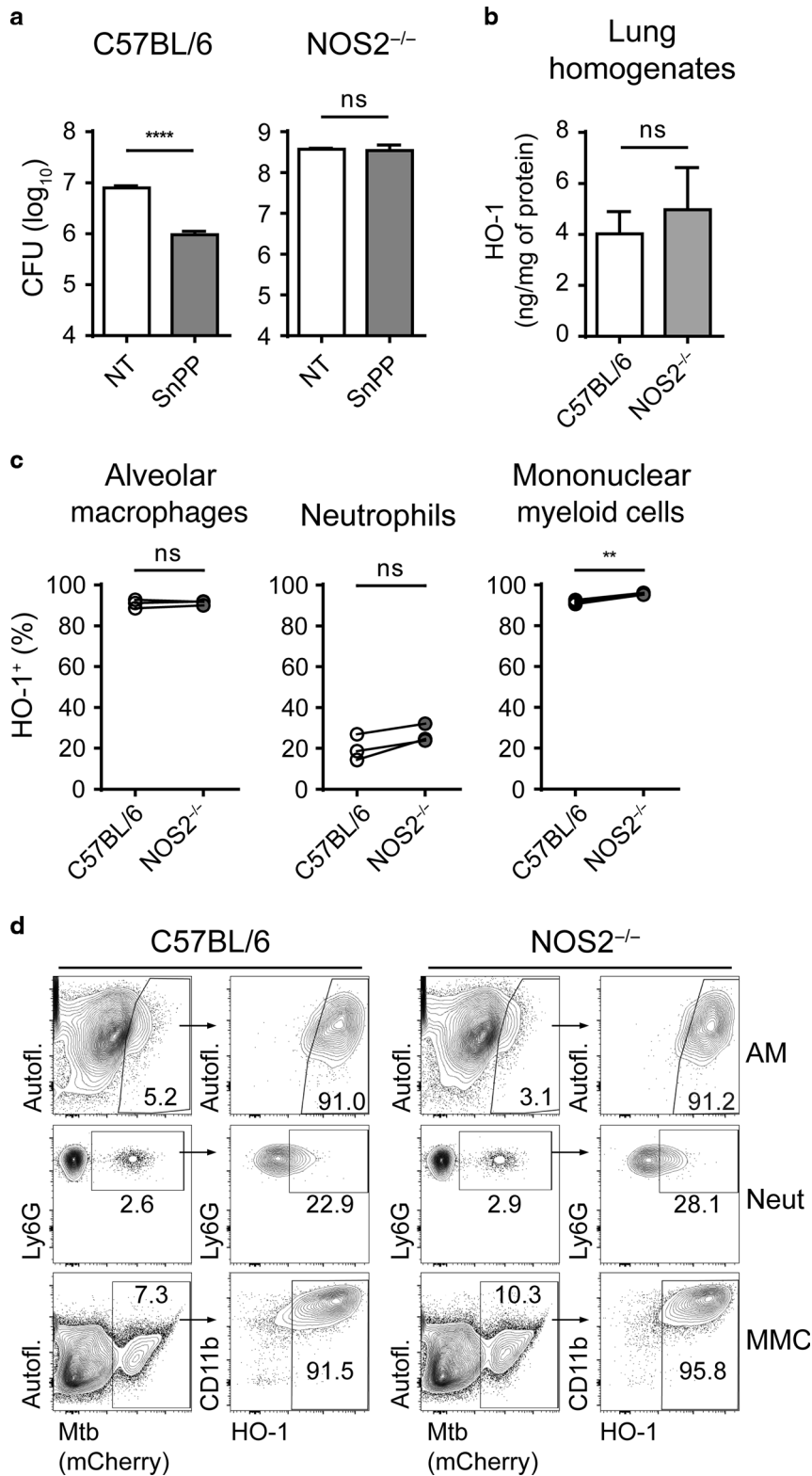
The bacterial load reduction resulting from SnPP treatment is dependent on host expression of NOS2  
The expression of NOS2 is upregulated in Mtb-infected macrophages and is further enhanced in response to IFN $\gamma$  activation (Fig. S5a). The resulting NO response plays a critical role in the control of murine Mtb infection<sup>16</sup> although multiple mechanisms may be involved.<sup>17</sup> As noted above, the upregulation of HO-1 protein expression in the lungs of Mtb-infected mice was found to be temporarily linked to the transcriptional expression of NOS2 in addition to IFN $\gamma$  (Fig. S2b). Moreover, we found that a major increase in NOS2 protein expression occurs in alveolar macrophages and parenchymal/alveolar mononuclear myeloid cells 20 days post infection with Mtb (Fig. S5b), a time point in which HO-1 expression also increases in the latter cell subset. To assess the involvement of NOS2 in the pharmacological effects of SnPP treatment, we infected C57BL/6 and NOS2<sup>-/-</sup> mice with Mtb and administered SnPP for 15 days starting at 4 wpi as described earlier. In contrast to the treated WT control animals, no bacterial load reduction was observed in NOS2<sup>-/-</sup> mice following SnPP administration (Fig. 4a), demonstrating a major requirement for NOS2 expression in the activity of the drug.

The role of NOS2 in SnPP function is not due to an effect on HO-1 expression in Mtb-infected myeloid cells  
The dependence of NOS2 expression for the HO-1 inhibition-induced reduction of bacterial burden in TB could reflect a role for NOS2 in the induction of HO-1 expression in Mtb-infected myeloid cells. In order to test this hypothesis, we first quantified HO-1 expression in lung homogenates of C57BL/6 and NOS2<sup>-/-</sup> mice and found no difference in enzyme levels between the two animal groups (Fig. 4b). In common with IFN $\gamma$ <sup>-/-</sup> mice, infected NOS2<sup>-/-</sup> animals developed a neutrophil-dominated pulmonary parenchymal and alveolar response (Fig. S5c, d). To rule this out as a complicating factor we also measured HO-1 expression by flow cytometry using the same mixed bone marrow chimera approach described above in which in this instance, CD45.1/2 WT mice were irradiated and adoptively transferred with equal numbers of WT (CD45.1) and NOS2<sup>-/-</sup> (CD45.2) bone marrow cells. We found that the Mtb-infected chimeric mice displayed similar levels of each myeloid subset in parenchyma and alveoli (Fig. S5e, f) and that Mtb infection was comparable in WT and NOS<sup>-/-</sup> neutrophils and

mononuclear myeloid cells from these compartments (Fig. S5g, h). In this normalized inflammatory niche, we analyzed parenchymal and alveolar myeloid cells and found no difference in HO-1 expression between WT and NOS2<sup>-/-</sup> Mtb-infected alveolar macrophages and neutrophils, while there was a slight but significant increase in the frequency of NOS2<sup>-/-</sup> HO-1<sup>+</sup> mononuclear myeloid cells compared to the WT population (Fig. 4c, d). These data confirmed that the dependence on NOS2 for the bacterial load reduction triggered by SnPP treatment is not due to a role for NOS2 in the induction of HO-1 expression.

SnPP treatment results in increased NOS2 expression and NO production by infected macrophages in response to IFN $\gamma$  activation  
The requirement for IFN $\gamma$  production and NOS2 expression for improved bacterial control following SnPP treatment could also be associated with a role for HO-1 in regulating NOS2 expression and NO production in response to IFN $\gamma$  activation of Mtb-infected cells. We used an in vitro approach in which C57BL/6 or NOS2<sup>-/-</sup> BMDM were infected with Mtb in the presence or absence of SnPP and/or IFN $\gamma$  to test this hypothesis. In C57BL/6 macrophages, SnPP-induced HO-1 inhibition alone induced a small, insignificant bacterial load reduction, while IFN $\gamma$  treatment alone as expected induced a major decrease in pathogen levels. Importantly, simultaneous treatment with SnPP and IFN $\gamma$  resulted in a highly significant further reduction in bacterial loads when compared to either SnPP or IFN $\gamma$  treatment alone. In direct contrast to C57BL/6 cells, in cultures employing NOS2<sup>-/-</sup> macrophages, no difference in bacterial numbers was found between cells treated or not with SnPP, either in the presence or in the absence of IFN $\gamma$  stimulation (Fig. 5a). We repeated this experiment using hemin as an inducer of HO-1 expression in C57BL/6 BMDM to test whether enhanced expression of the enzyme might impair bacterial replication control. We found that the bacterial loads were similar between nontreated and hemin-treated cells. Also, the reduction in the number of bacteria resulting from IFN $\gamma$  treatment remained unchanged when hemin was included with the cytokine. As expected, the additional supplementation of SnPP to the IFN $\gamma$  and hemin-treated cultures, resulted in further reduction of bacterial loads (Fig. S6a). These data suggest that increasing HO-1 expression beyond that induced by Mtb infection does not impair bacterial replication control by macrophages in vitro.

We also assessed NOS2 expression by flow cytometry and quantified nitrite by Griess assay in the supernatants as a readout of NO production. We observed significantly increased expression of NOS2 in SnPP-treated macrophages activated with 10 and 100 U/mL of IFN $\gamma$  (Fig. 5b, c) as well as higher NO production in macrophage cultures in the simultaneous presence of IFN $\gamma$  and SnPP (Fig. 5d). These data argued that SnPP-mediated HO-1 inhibition enhances NOS2 expression and NO production in Mtb-infected IFN $\gamma$ -activated macrophages, resulting in improved bacterial control.



The enhanced bacterial control resulting from pharmacological inhibition of HO-1 in IFN $\gamma$ -activated macrophages is associated with a reduction in intracellular iron levels. HO-1 catalyzes a critical step in heme degradation that results in the generation of equimolar amounts of carbon monoxide (CO), biliverdin, and iron.<sup>18</sup> These products can each have immunopharmacological effects in hematopoietic cells that can potentially

affect host resistance to infection.<sup>19</sup> In order to evaluate if the outcome of pharmacological HO-1 inhibition in IFN $\gamma$  activated Mtb-infected macrophages stems from the reduced generation of any of these products, we treated these cells with either a CO donor (CORM2), biliverdin (biliverdin hydrochloride), or iron (FeSO<sub>4</sub>), to evaluate if any of these agents could reverse the effects of SnPP treatment. Treatment with the compounds alone

**Fig. 4 NOS2 expression is required for the bacterial load reduction mediated by pharmacologic HO-1 inhibition in vivo.** **a** CFU loads in lung homogenates of C57BL/6 and NOS2<sup>-/-</sup> Mtb-infected mice treated or not for 15 days with SnPP ( $n = 3$  mice/group). **b** HO-1 quantification by ELISA in lung homogenates obtained from C57BL/6 and NOS2<sup>-/-</sup> mice at 4 weeks post infection (wpi) with Mtb ( $n = 4$  and 3 mice/group). **c** HO-1 expression measured by flow cytometry in mCherry Mtb<sup>+</sup> donor alveolar macrophages (AM), parenchymal neutrophils (Neut), or parenchymal myeloid mononuclear cells (MMC) recovered from the lungs of infected receptor mice at 4 wpi and gated as detailed in Fig. S1 (bone marrow chimeras were generated as described for Fig. 2f, but reconstituted with bone marrow from B6/SJL (CD45.1) and NOS2<sup>-/-</sup> (CD45.2) mice) ( $n = 3$  mice/group). **d** Representative dot plots from data depicted in Fig. 4c, showing gating of Mtb<sup>+</sup> cells in left-hand panels and HO-1 expression in gated cells in right-hand panels flow cytometry data concatenated from three samples). Data expressed as mean  $\pm$  standard error of mean (**a** and **b**), paired individual samples (**c**), or dot plots from concatenated data (**d**). Data shown are representative of two (**b-d**) or three (**a**) independent experiments. Statistical analyses: unpaired (**a** and **b**) and paired (**c**) Student's  $t$  test. \*\* $p < 0.01$ , \*\*\*\* $p < 0.0001$ , n.s. nonsignificant.

or in combination with IFN $\gamma$  in the absence of SnPP did not result in significant changes in bacterial levels in vitro (Fig. S6b). However, in macrophages treated with SnPP plus IFN $\gamma$ , we found that the addition of iron reversed the bacterial load reduction resulting from HO-1 inhibition, while no effect was observed following the addition of either the CO donor or biliverdin (Fig. 6a). We also found that NOS2 expression in IFN $\gamma$ -activated Mtb-infected macrophages, which increased with SnPP treatment, was lower in the presence of iron (Fig. 6b, c). A similar effect of iron supplementation was observed on the levels of NO produced by these cells, which were higher in the presence of SnPP, but returned to levels comparable to those expressed by IFN $\gamma$  treated cells in the absence of the HO-1 inhibitor (Fig. 6d). As a control, we also treated IFN $\gamma$  activated Mtb-infected macrophages with an iron-chelating agent and as expected found an increase in NOS2 expression, both in the absence and presence of iron supplementation (Fig. S6c).

We next asked whether SnPP-induced HO-1 inhibition results in reduced intracellular iron in Mtb-infected cells using an assay for intracellular labile iron based on calcein-AM staining.<sup>20</sup> We found that SnPP-induced HO-1 inhibition in IFN $\gamma$ -activated Mtb-infected BMDM in vitro results in a significant decrease in intracellular iron levels (Fig. 6e). To assess whether SnPP treatment induces a similar reduction in iron levels in vivo, we performed Perls staining followed by diaminobenzidine (DAB) enhancement (Perls-DAB) to detect iron in lung sections from Mtb-infected mice treated or not with SnPP. By analyzing areas with infiltration of inflammatory cells, we found enhanced iron detection by Perls-DAB staining in lungs of nontreated mice compared to those of SnPP-treated animals (Fig. 7a, b). Furthermore, the levels of ferritin, an iron-chelating protein whose expression is induced in response to heightened cytosolic levels of the metal,<sup>5,18</sup> were substantially reduced in lung homogenates as well as in sorted Mtb-infected pulmonary myeloid cells from SnPP-treated mice in comparison with those of untreated animals (Fig. 7c). Based on these results, we propose a mechanism (Fig. 8) in which SnPP-mediated inhibition of HO-1 activity in Mtb-infected cells results in reduced intracellular iron levels that in addition to its predicted effects in restricting pathogen growth, enhances the control of bacterial replication mediated by IFN $\gamma$ -dependent NO production.

## DISCUSSION

HO-1 is a host enzyme that is strongly regulated by Mtb infection in humans and experimental models and its role in most studies has been linked to its antioxidant functions.<sup>21</sup> Whether the function of HO-1 in Mtb infection is purely host protective is a subject of controversy. Thus, mice totally or conditionally genetically deficient in HO-1 are more susceptible to chronic Mtb infection,<sup>22</sup> although in the case of the total HO-1 knockout animals this finding is complicated by baseline alterations in the myeloid lineage probably resulting from heme toxicity.<sup>23</sup> On the other hand, in vitro studies employing HO-1 enzymatic inhibitors or knockdown of the HO-1 gene support a mycobacterium promoting role for the molecule. Thus, Mtb-infected human or as

shown here (Fig. 5a) mouse macrophages show enhanced control of bacterial growth when treated with SnPP<sup>12</sup> as do human THP-1 cells knocked down for HO-1 when infected with *Mycobacterium abscessus*.<sup>24</sup> In addition, as previously reported by us, SnPP-treated mice show highly significant and reproducible reductions in pulmonary bacterial loads, which in the first 3 weeks of administration are indistinguishable from those achieved with conventional antibiotic treatment.<sup>8</sup> It is highly unlikely that these antibacterial outcomes of SnPP treatment represent a direct effect on the pathogen, since SnPP fails to restrict bacterial growth in the absence of host adaptive immunity in vivo (Figs. 3 and 4) or in liquid bacterial culture.<sup>8,12,24</sup> Instead, we speculate that the contrary outcomes of HO-1 suppression in these multiple studies reflect the difference between temporary versus chronic absence of the enzyme itself or in the case of SnPP treatment, its activity. In this regard, it has been demonstrated in silico that the HO-1 protein can serve as a scaffold for a variety of biologically important molecules<sup>25</sup> and consequently as suggested in a recent study<sup>26</sup> that the enzyme may have additional functions beyond heme degradation itself. Such secondary activities would be absent in HO-1 deficient mice and thus could provide an indirect explanation for the impaired resistance of these animals to mycobacterial infection seen in previous studies.

In the present report, we investigated the immune dependence of SnPP treatment on Mtb infection and as a first step in doing so, characterized the source of the enzyme in our murine model. Myeloid cells and in particular splenic and liver macrophages have been traditionally considered to be the major site of HO-1 function because of the enzyme's role in recycling iron from senescent red blood cells.<sup>27</sup> Nevertheless, it is only recently that the HO-1-producing myeloid subsets in other tissue sites have been characterized.<sup>28,29</sup> In the current study we found that in mice, inflammatory monocyte derived macrophages are the major source of HO-1 in Mtb-infected lungs, with a minor contribution from alveolar macrophages, in the parenchymal and alveolar compartments. Importantly, we determined that while most of the HO-1 is derived from uninfected cells, essentially all Mtb-infected cells produce the enzyme. This observation that is consistent with in vitro findings from a previous study<sup>12</sup> indicates that in vivo HO-1 expression always accompanies Mtb intracellularly where it is appropriately situated to affect pathogen survival/growth.

We have previously shown that the activity of SnPP on Mtb infection is defective in TCR $\alpha$ <sup>-/-</sup> mice that lack functional conventional  $\alpha\beta$  T cells.<sup>8</sup> In the present study, we have extended these observations by demonstrating a key role for the major Th1 effectors IFN $\gamma$  and NOS2 in this immune dependence consistent with the known kinetics of the Mtb-restricting Th1 response in infected mice and the corresponding delay in the responsiveness of these animals to SnPP treatment. Our data argue that the dependence of SnPP efficacy on IFN $\gamma$  and NO is not due to a role for these effectors in either HO-1 induction or suppression of IFN $\gamma$  production by HO-1. Instead, we favor the hypothesis that the induction of HO-1 expression in Mtb-infected cells suppresses IFN $\gamma$ -dependent NOS2 and NO production, thus promoting bacterial survival and growth.



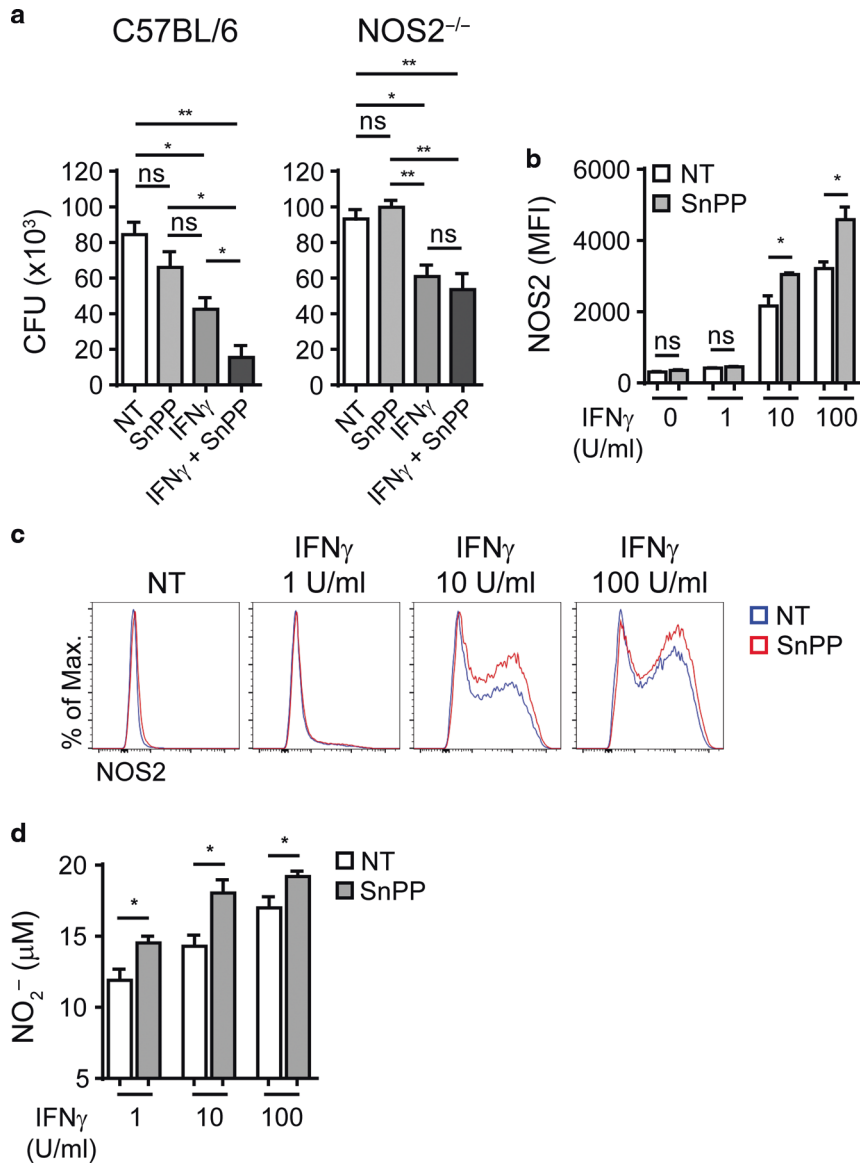


**Fig. 5** The effect of HO-1 inhibition on intracellular bacterial levels in vitro is dependent on both IFN $\gamma$  and NOS2 expression. **a** CFU loads obtained from C57BL/6 or NOS2<sup>-/-</sup> BMDM 96 h post infection and stimulation or not with IFN $\gamma$  (250 U/mL), SnPP (1  $\mu$ M), or IFN $\gamma$  (250 U/mL) plus SnPP (1  $\mu$ M) (triplicates). **b** NOS2 expression quantified in C57BL/6 BMDM by flow cytometry 24 h post infection and stimulation or not with IFN $\gamma$  (1, 10, or 100 U/mL) in the presence or absence of SnPP (1  $\mu$ M) (triplicates). **c** Representative histograms of data shown in Fig. 5b (flow cytometry data concatenated from triplicates). **d** Nitrite concentration quantified in supernatants of C57BL/6 BMDM 24 h post infection and stimulation with IFN $\gamma$  (1, 10, or 100 U/mL) in the presence or absence of SnPP (1  $\mu$ M) (triplicates). Data expressed as mean  $\pm$  standard error of mean (**a**, **b**, and **d**) or histograms from concatenated data (**c**). Data shown are representative of two (**a**–**c**) or three (**d**) independent experiments performed in triplicates. \* $p$  < 0.05, \*\* $p$  < 0.01, n.s. nonsignificant.

In contrast to our findings, a recent study by Singh et al.<sup>30</sup> employing IFN $\gamma$ -treated RAW264.7 cells reported that SnPP treatment impairs rather than promotes the control of Mtb infection in vitro. The authors attributed this outcome to an effect of the CO generated as a result of HO-1 activity in promoting IFN $\gamma$ -induced autophagic control of bacterial replication<sup>30</sup> but did not confirm the effects of SnPP on bacterial control or the role of this proposed HO-1 regulated autophagic pathway in vivo. At present the basis of the discordant in vitro effects of SnPP treatment on bacterial growth observed here and in the previous study by Singh et al. are unclear but may relate to the different host cells (BMDMs versus RAW tumor cells) employed.

A role for HO-1 in suppressing reactive nitrogen species production has also been proposed in human TB based on analysis of diseased versus nondiseased lung sections.<sup>28</sup> However,

in apparent contrast to our hypothesis, the authors of that study interpreted their findings as evidence for a protective role of HO-1 in preventing chronic tissue damage. Nevertheless, their observations do not exclude the existence of a beneficial effect of short-term suppression of the HO-1 activity in promoting bacterial control through the same mechanism of NO production enhancement. Such a host protective function might be of particular relevance in the context of adjunctive HDT where a HO-1 inhibitor such as SnPP would be administered in conjunction with conventional antibiotics.

The antioxidant and anti-inflammatory activities of HO-1 are usually attributed to its generation of biliverdin (and subsequently bilirubin) and CO respectively from heme.<sup>21</sup> Biliverdin and bilirubin scavenge superoxide (O $_2^-$ ) and peroxynitrite (ONOO $^-$ ), a toxic metabolite resulting from the reaction of NO with O $_2^-$ ,<sup>31</sup>

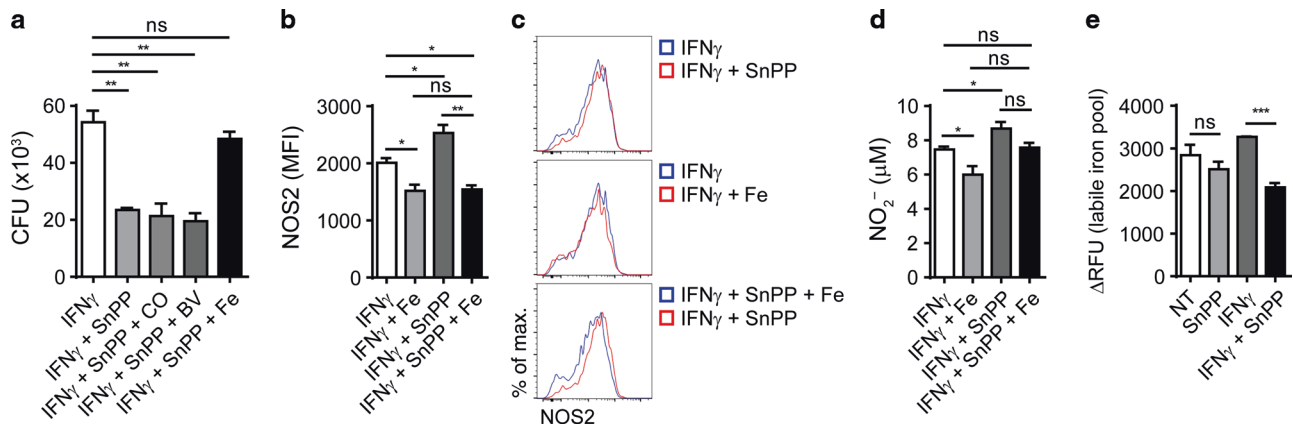


**Fig. 6 The effects of HO-1 inhibition on IFN $\gamma$ -mediated control of intracellular bacterial levels correlate with intracellular iron levels.** **a** CFU loads obtained from C57BL/6 BMDM 96 h post infection and stimulation with IFN $\gamma$  (250 U/mL), IFN $\gamma$  (250 U/mL) plus SnPP (1  $\mu$ M), IFN $\gamma$  (250 U/mL) plus SnPP (1  $\mu$ M) plus CORM2 (5  $\mu$ M)—IFN $\gamma$  + SnPP + CO, IFN $\gamma$  (250 U/mL) plus SnPP (1  $\mu$ M) plus biliverdin (5  $\mu$ M)—IFN $\gamma$  + SnPP + BV, or IFN $\gamma$  (250 U/mL) plus SnPP (1  $\mu$ M) plus FeSO $_4$  (5  $\mu$ M)—IFN $\gamma$  + SnPP + Fe (triplicates). **b** NOS2 expression in C57BL/6 BMDM 24 h post infection and stimulation with IFN $\gamma$  (100 U/mL), IFN $\gamma$  (100 U/mL) plus SnPP (1  $\mu$ M), or IFN $\gamma$  (100 U/mL) plus SnPP (1  $\mu$ M) plus FeSO $_4$  (5  $\mu$ M)—IFN $\gamma$  + SnPP + Fe (triplicates). **c** Representative dot plots of data shown in Fig. 6b (flow cytometry data concatenated from triplicates). **d** Nitrite levels in supernatants of C57BL/6 BMDM infected and stimulated as in Fig. 6b (triplicates). **e** Labile iron pool readout measured as  $\Delta$ RFU (relative fluorescence units) in BMDM lysates 24 h post infection and stimulation or not with IFN $\gamma$  (250 U/mL), SnPP (1  $\mu$ M), or IFN $\gamma$  (250 U/mL) plus SnPP (1  $\mu$ M) (triplicates). The data are presented as the means  $\pm$  standard error (**a**, **b**, **d**, and **e**) or histograms from concatenated data (**c**). Data shown are representative of two (**a–e**) independent experiments. Statistical analysis: Student's *t* test. \**p* < 0.05, \*\**p* < 0.01, \*\*\**p* < 0.001, n.s. nonsignificant.

while CO triggers signaling pathways that culminate in decreased production of TNF in macrophages,<sup>32</sup> a pro-inflammatory cytokine known to induce NOS2 expression.<sup>33</sup> However, in the experiments presented here the addition of either biliverdin or CO to IFN $\gamma$ -activated Mtb-infected macrophages failed to inhibit the enhanced NOS2-dependent reduction in bacterial loads resulting from SnPP treatment. Instead, it was only the addition of iron, the third enzymatic product of HO-1 activity, that reverted the effects of SnPP in the latter in vitro system and this outcome was associated with a corresponding reduction in NOS2 expression and NO production. Moreover, we observed that SnPP treatment results in reduction of intracellular iron levels in Mtb-infected macrophages in vitro and we provide correlative evidence supporting a role for this effect in vivo. HO-1 activity has been suggested to mediate intracellular iron accumulation in vivo in LPS-induced septic shock<sup>34</sup> and it was demonstrated that the iron overload found in experimental liver fibrosis could be reverted by pharmacological inhibition of the enzyme.<sup>35</sup> These previously published observations support our own findings indicating that the enhanced HO-1 activity triggered by Mtb infection associates with iron overload in vivo and suggesting that this upregulation of intracellular iron levels results in impaired IFN $\gamma$ -induced NOS2-NO production thereby promoting pathogen survival. The latter conclusion is consistent with previous findings demonstrating that iron suppresses IFN $\gamma$  and LPS-induced NO production by macrophages.<sup>36</sup> Further experiments causally linking Mtb induced HO-1 activity, increased iron levels and decreased NO response are needed to firmly establish the existence of this regulatory pathway in vivo.

Fluctuations in iron levels have been long believed to influence the outcome of Mtb infection.<sup>37</sup> This association in most cases has been linked with the well-known nutritional effects of iron on mycobacterial growth,<sup>6,11</sup> a mechanism that is not universally agreed upon (e.g., Harington-Kandt et al.<sup>38</sup>). We have previously shown that excessive iron accumulation in Mtb-infected cells can induce necrotic cell death by ferroptosis, promoting tissue damage and favoring bacterial dissemination.<sup>39</sup> Whether iron derived from heme degradation contributes to this process remains to be formally investigated along with the possible

function of ferroptosis inhibition in the therapeutic effects of SnPP in vivo. Instead, the present study provides evidence for the role of iron resulting from HO-1 enzymatic activity in promoting survival of this pathogen through its activity in suppressing a major antimycobacterial effector, NO, by means of its known property as an inhibitor of NOS2.<sup>36,40,41</sup> The precise mechanism by which iron regulates NOS2 synthesis has not been fully elucidated. It has been demonstrated that iron impairs the binding capacity of the NF-IL6 (C/EBP $\beta$ ) transcription factor to the *Nos2* gene promoter region thereby reducing IFN $\gamma$ -induced NOS2 protein expression.<sup>42</sup> A second mechanism that has been previously proposed involves the known property of iron as a cofactor for the activation of the enzyme prolyl hydroxylase (PHD), which in turn degrades HIF1 $\alpha$ ,<sup>43,44</sup> a major inducer of NOS2 expression.<sup>45</sup> In this scenario, SnPP by inhibiting the generation of iron from heme would suppress PHD activity and consequently enhance HIF1 $\alpha$ -mediated NOS2 production and bacterial control. Alternatively, as observed in in vitro *S. typhimurium* infection, iron accumulation could also enhance the production of the anti-inflammatory cytokine IL-10, which can suppress NOS2 expression.<sup>46</sup> Whether the reduction in intracellular iron levels triggered by SnPP treatment also contributes to its effects by decreasing the levels of the metal required as a nutrient for pathogen growth remains to be determined.

Importantly, our previous and ongoing studies indicate SnPP treatment as a successful and highly reproducible therapy for TB in experimental murine infection. In recent work (Adeleke et al. unpublished), we have been able to formulate the drug as a prolonged release intramuscular injection feasible for clinical use. Although never assessed for its effect on human TB, SnPP has been previously used clinically for the treatment of jaundice in infants<sup>47,48</sup> and has been tested experimentally as a therapy for porphyria.<sup>49,50</sup> The most common side effect associated with its use is a transient phototoxicity.<sup>51</sup> Although HO-1 plays an important role in iron metabolism, acute treatment with SnPP does not result in iron deficiency anemia,<sup>52</sup> but this side effect has been observed during chronic administration of tin mesoporphyrin (another tin based porphyrin HO-1 inhibitor), but was reversed after cessation of treatment.<sup>53</sup> In addition to repurposing SnPP,

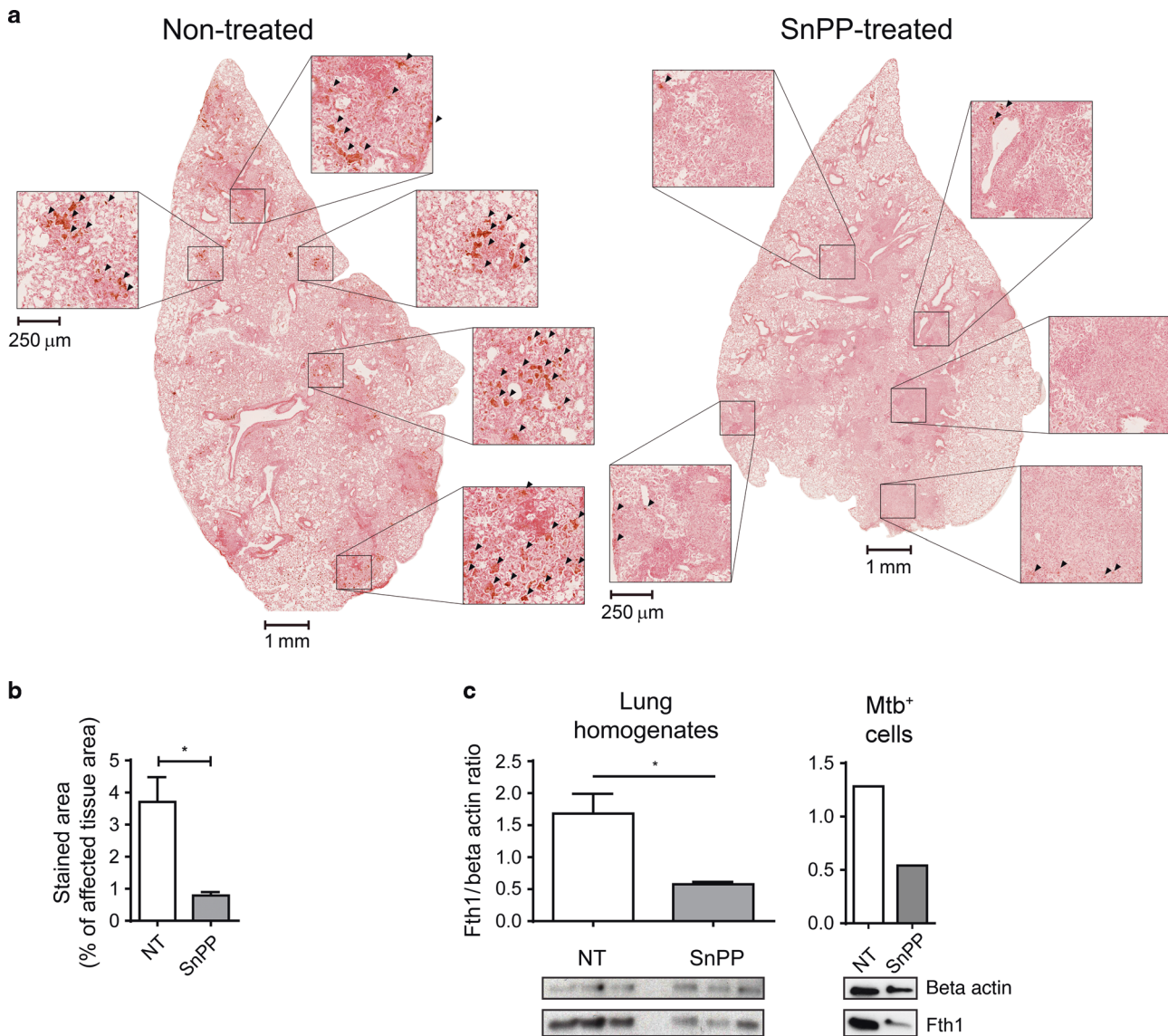


**Fig. 7 Pharmacological HO-1 inhibition results in decreased iron accumulation in lungs of Mtb-infected mice.** **a** Photomicrographs of whole lung lobes (1 mm scale bars) and magnified fields (250  $\mu$ m scale bars) showing Perls-DAB staining in histological sections of lungs of Mtb-infected C57BL/6 mice that were treated or not with SnPP for 21 days starting at 28 days post infection (dpi)—arrowheads indicate areas with positive Perls-DAB staining. **b** Graphs showing percentage represented by Perls-DAB positively stained area in regions containing infiltration of inflammatory cells, in histological sections from lungs of Mtb-infected C57BL/6 mice treated or not SnPP for 21 days starting at 28 dpi ( $n = 4$  and 3 mice/group). **c** Graphs showing quantification of ferritin heavy chain (Fth1) expression normalized to that of beta actin (endogenous control) (top) and images of western blot membrane showing Fth1 and beta actin expression (bottom) in lung homogenates (left) and mCherry Mtb<sup>+</sup> pulmonary leukocytes isolated by sorting (right) from C57BL/6 Mtb-infected mice treated or not with SnPP for 21 days starting at 28 days post infection ( $n = 3$  mice/group on left panel and pooled samples from 3 mice/group in right panel). The data are presented as the means  $\pm$  standard error (**b** and **c**), photomicrographs of individual samples (**a**), or individual samples (**c**). Data shown are representative of two independent experiments. Statistical analysis: Student's  $t$  test. \* $p < 0.05$ .

other HO-1 inhibitors exist or are in development (e.g., imidazole-dioxolane derivatives) that could be experimentally tested for their therapeutic effect on Mtb infection.<sup>54</sup> As emphasized here, as well as in our previous study,<sup>8</sup> the effects of HO-1 inhibition by SnPP are T-cell dependent and this may limit the efficacy of the drug in HIV-TB patients with lowered CD4<sup>+</sup> T lymphocyte counts. On the other hand, the immune dependence of SnPP therapy raises the interesting counter question of whether an HO-1 inhibitor might enhance bacterial clearance when used as an adjunct to therapeutic vaccination<sup>55,56</sup> of individuals with established infections. At a more general level, the results reported here underscore the importance of iron metabolism as a potential

target for intervention in TB both at the levels of the pathogen and the host-defense mechanisms to which it is susceptible.

#### METHODS

Experimental animals and in vivo bacterial infections  
C57BL/6J, B6.SJL, C57BL/6J  $\times$  B6.SJL F1, IFN $\gamma$ <sup>-/-</sup>, TCR $\alpha$ <sup>-/-</sup>, IFN $\gamma$ R<sup>-/-</sup>, and NOS2<sup>-/-</sup> mice were obtained through a National Institute of Allergy and Infectious Diseases (NIAID) supply contract with Taconic Farms (Germantown, NY), or purchased from The Jackson Laboratory (Bar Harbor, ME). All animals were housed at BSL-2 and BSL-3 animal facilities at the NIAID, National Institutes of

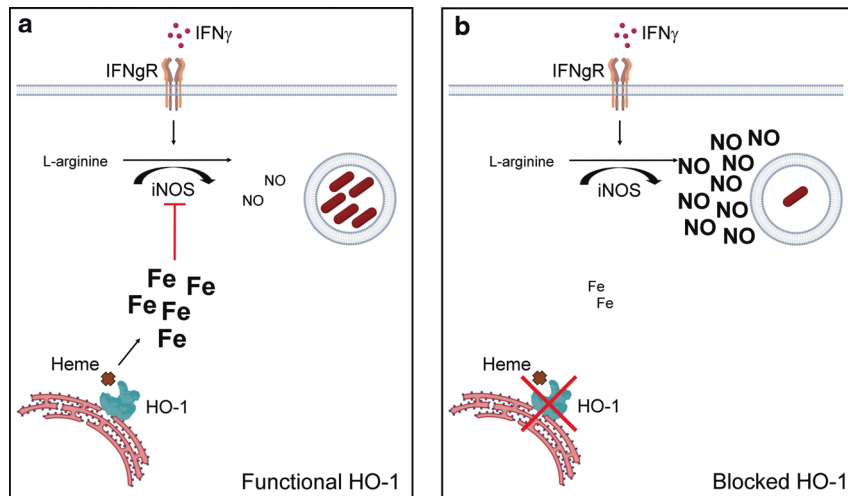


**Fig. 8 Proposed mechanisms for effect of HO-1 enzymatic inhibition on control of Mtb infection.** **a** *M. tuberculosis* infection induces HO-1 expression which catalyzes heme degradation and increases intracellular iron levels. This in turn suppresses NOS2-dependent NO production induced by IFN $\gamma$  activation. **b** Inhibition of HO-1 with SnPP results in reduced free iron levels in *M. tuberculosis*-infected cells thereby enhancing IFN $\gamma$  dependent NOS2-induced NO production and bacterial control.

Health (NIH), and all the experimental protocols were approved by the NIAID Animal Care and Use Committee. Mice were aerosol-infected with ~100 CFU of Mtb strain H37Rv or a H37Rv strain transformed with an mCherry reporter plasmid driven by the pMSP12 promoter<sup>57</sup> in whole body exposure/inhalation system (Glas Col, Terre Haute, IN). Bacterial loads were quantified in organ homogenates through a limiting dilution assay utilizing 7H11 agar medium (Sigma-Aldrich, Saint Louis, MO) enriched with OADC (BD Biosciences, San Jose, CA).

#### BMDM cultures and in vitro infection

For BMDM generation, marrow was obtained from femurs and tibia and cultured in Petri dishes (100×15 mm) containing 10 mL of DMEM/F-12 (Gibco, Thermo Fisher Scientific, Waltham, MA) differentiation medium as described previously.<sup>39</sup> The cells were next seeded in flat bottom 96-well plates in RPMI medium (Gibco, Thermo Fisher Scientific, Waltham, MA) at a concentration of  $8 \times 10^4$  cells/well, allowed to adhere overnight and exposed to Mtb strain H37Rv at a multiplicity of infection of 3 (MOI:3) for 4 h after which noninternalized bacteria were removed by washing and different stimuli were added. For bacterial load quantification, BMDM were lysed for 10 min in PBS containing 0.05% (w/v) of saponin and a limiting dilution colony count performed with the cell lysates as described above.

#### SnPP, CORM2, biliverdin, and iron sulfate treatment

For all in vivo tin protoporphyrin IX (SnPP) (Frontier Scientific, Logan, UT) treatments, mice were intraperitoneal injected daily (5 mg/kg/mouse in 200  $\mu$ L of PBS) starting 28 days post infection. In vitro, SnPP was added to culture medium for at a concentration of 1  $\mu$ M. In in vitro experiments, biliverdin hydrochloride (Frontier Scientific, Logan, UT), Tricarbonyldichlororuthenium II (CORM2), or FeSO<sub>4</sub> (both from Sigma-Aldrich, Saint Louis, MO) were added to cell culture medium all at 5  $\mu$ M.

#### Pulmonary cell isolation

Mice were euthanized by cervical dislocation following anesthesia by isoflurane inhalation. Lungs were perfused with PBS prior to excision. Lungs and spleens were incubated for 40 min at 37 °C in digestion medium (RMPI (Gibco, Thermo Fisher Scientific, Waltham, MA) + collagenase IV (100 U/mL) + DNase I (50 U/mL) (both from Sigma-Aldrich, Saint Louis, MO)), after which they were mashed through 100  $\mu$ m nylon strainers. Viable cell concentrations were determined by microscopic counting on Neubauer chambers in the presence of trypan blue.

#### Flow cytometry

For ex vivo flow cytometric analyzes, mice were intravenously injected with a solution containing 1  $\mu$ g of anti-mouse CD45 antibody and 10 U of heparin, 3 min prior to euthanasia. Single-cell suspensions from harvested organs or from BMDM cultures were labeled with a fixable viability dye (Thermo Fisher Scientific, Waltham, MA) and then with fluorochrome-conjugated antibodies specific for cell surface markers. For intracellular staining, cells were further permeabilized by utilizing a Cytofix/Cytoperm™ kit (BD Biosciences, San Jose, CA) or with an eBioscience FoxP3/Transcription Factor Staining Buffer Set™ (Thermo Fisher Scientific, Waltham, MA) prior to addition of specific antibodies. The antibodies used are depicted in Table S1. LSRFortessa and FACSymphony flow cytometers (BD Biosciences, San Jose, CA) were used in cell acquisition. Data were analyzed utilizing FlowJo software (FlowJo LLC, Ashland, OR).

#### Quantification of mRNA expression by real-time PCR

Perfused lungs from naive and Mtb-infected mice were disrupted in 2 mL tubes containing 2.7 mm glass beads and Trizol reagent (Thermo Fisher Scientific, Waltham, MA) using a Precellys Evolution™ tissue homogenizer (Bertin Instruments, Montigny-le-Bretonneux, France). mRNA was extracted from samples utilizing Qiagen RNeasy mini kits (Qiagen, Hilden, Germany) and Direct-zol™ RNA mini-prep kits (Zymo Research, Irvine, CA). One microgram of RNA was then reverse transcribed into cDNA using superscript II reverse transcriptase and random primers (Thermo Fisher Scientific, Waltham, MA). SYBR Green, 7900HT Fast Real-Time PCR, and Quant-Studio 7 Real-Time PCR Systems (Applied Biosystems, Thermo Fisher Scientific, Waltham, MA) were employed for real-time PCR reactions. Relative expression of genes of interest in Mtb-infected mouse lungs was calculated using the  $\Delta\Delta$  cycle threshold method. mRNA expression in each sample was normalized to that of  $\beta$ -actin and further analyzed in relation to those of uninfected naive mice lungs. Murine primers used: Actb F: 5' AGC TGC GTT TTA CAC CCT TT 3'; Actb R: 5' AAG CCA TGC CAA TGT TGT CT 3'; Hmox1 F: 5' GCC ACC AAG GAG GTA CAC AT 3'; Hmox1 R: 5' GCT TGT TGC GCT CTA TCT CC 3'.

#### Immunoassays

Perfused lungs from naive and Mtb-infected mice were disrupted in 2 mL tubes containing 2.7 mm glass beads and PBS with cComplete ULTRA™ protease inhibitor cocktail (Roche, Basel, Switzerland) and 2 mM of PMSF (Sigma-Aldrich, Saint Louis, MO),

using a Precellys Evolution<sup>TM</sup> tissue homogenizer (Bertin Instruments, Montigny-le-Bretonneux, France). Cell cultures were lysed in Cell Lysis Buffer (Cell Signaling Technology, Danvers, MA) containing cComplete ULTRA<sup>TM</sup> protease inhibitor cocktail (Roche, Basel Switzerland) and 2 mM of PMSF (Sigma-Aldrich, Saint Louis, MO). For western blot, samples were denatured for 5 min at 95 °C in reducing buffer (Thermo Fisher Scientific, Waltham, MA), separated in mini-protean TGX gels (Bio-Rad, Hercules, CA) and transferred to PVDF membranes prior to staining with specific antibodies and development with luminol. Protein expression in samples was calculated utilizing ImageJ software in relation to  $\beta$ -actin expression. The concentration of HO-1 in samples was measured by ELISA using mouse HO-1 ELISA set (Enzo Life Sciences, Farmingdale, NY). Antibody specifications are provided in Table S1.

Labile iron concentration measurement and Perls staining of iron in tissues

For the quantification of intracellular labile iron concentration, we used a modified calcein-AM staining protocol as described previously in which intracellular labile iron concentration is determined by the difference between calcein-AM fluorescence values of a sample incubated in the presence and absence of an iron-chelating agent.<sup>20</sup> Briefly, samples of BMDM lysate (lysed for 10 min in PBS containing 0.05% of saponin) were incubated for 15 min at room temperature with 250  $\mu$ M of deferoxamine mesylate (DFO) or PBS, followed by staining with calcein-AM (Thermo Fisher Scientific, Waltham, MA) at 125 nM for 30 min at 37 °C, in opaque 96-well plates (Corning, Corning, NY). Relative fluorescence units (RFU) were measured and labile iron levels are represented as  $\Delta$ RFU (DFO-treated sample RFU minus PBS treated sample RFU). Perls staining followed by DAB enhancement was performed by Histoserv, Inc. (Germantown, MD, USA) in histological sections from Mtb-infected mouse lungs previously fixed in PBS buffer containing 10% formalin, as described elsewhere.<sup>58</sup> Images were acquired in an Aperio Digital Pathology Slide Scanner (Leica, Buffalo Grove, IL, USA) and analyzed using ImageScope (Leica, Buffalo Grove, IL, USA) and ImageJ<sup>59</sup> software.

Statistical analyses

Differences between groups were statistically evaluated by paired and unpaired Student's *t* test using Prism software (GraphPad) and considered significant when  $p \leq 0.05$ .

## ACKNOWLEDGEMENTS

The authors would like to thank Sandra Oland and the staff from the NIAID animal facilities for technical assistance and Dr. Dragana Jankovic, Dr. Daniel Barber, and Dr. Katrin Mayer-Barber for scientific discussion during manuscript preparation. This work was supported by the Intramural Research Program of the NIAID, NIH. This work was financially supported by the Intramural Research Program of the NIAID, NIH.

## AUTHOR CONTRIBUTIONS

Conceptualization: D.L.C. and A.S.; experimental design: D.L.C., E.P.A., B.B.A., and A.S.; investigation: D.L.C., E.P.A., S.N., L.R.M., L.F., C.C.B., A.S.-S., and S.E.H.; data analysis and interpretation: D.L.C., E.P.A., S.N., B.B.A., R.W.T., and A.S.; resources: A.S.; writing: original draft—D.L.C. and A.S.; review and editing: D.L.C., E.P.A., S.N., B.B.A., and A.S.; supervision: A.S.; and funding acquisition: A.S.

## ADDITIONAL INFORMATION

The online version of this article (<https://doi.org/10.1038/s41385-020-00342-x>) contains supplementary material, which is available to authorized users.

**Competing interests:** The authors declare no competing interests.

**Publisher's note** Springer Nature remains neutral with regard to jurisdictional claims in published maps and institutional affiliations.

## REFERENCES

1. WHO. *Global Tuberculosis Report 2018*. (World Health Organization, Geneva, Switzerland, 2018).
2. Keshavjee, S. & Farmer, P. E. Tuberculosis, drug resistance, and the history of modern medicine. *N. Engl. J. Med.* **367**, 931–936 (2012).
3. WHO. *Guidelines for Treatment of Tuberculosis* 4th edn. (WHO Press, Geneva, Switzerland, 2010).
4. Young, C., Walz, G. & Du Plessis, N. Therapeutic host-directed strategies to improve outcome in tuberculosis. *Mucosal Immunol.* **13**, 190–204 (2020).
5. Gozzelino, R. & Soares, M. P. Coupling heme and iron metabolism via ferritin H chain. *Antiox. Redox Signal.* **20**, 1754–1769 (2014).
6. Wells, R. M. et al. Discovery of a siderophore export system essential for virulence of *Mycobacterium tuberculosis*. *PLoS Path.* **9**, e1003120 (2013).
7. Ganz, T. & Nemeth, E. Iron homeostasis in host defence and inflammation. *Nat. Rev. Immunol.* **15**, 500–510 (2015).
8. Costa, D. L. et al. Pharmacological inhibition of host heme oxygenase-1 suppresses *Mycobacterium tuberculosis* infection in vivo by a mechanism dependent on T lymphocytes. *mBio* **7**, e01675–16 (2016).
9. Ernst, J. D. The immunological life cycle of tuberculosis. *Nat. Rev. Immunol.* **12**, 581–591 (2012).
10. Dawson, R. et al. Immunomodulation with recombinant interferon-gamma1b in pulmonary tuberculosis. *PLoS ONE* **4**, e6984 (2009).
11. De Voss, J. J. et al. The salicylate-derived mycobactin siderophores of *Mycobacterium tuberculosis* are essential for growth in macrophages. *Proc. Natl Acad. Sci. USA* **97**, 1252–1257 (2000).
12. Scharn, C. R. et al. Heme oxygenase-1 regulates inflammation and mycobacterial survival in human macrophages during *Mycobacterium tuberculosis* infection. *J. Immunol.* **196**, 4641–4649 (2016).
13. Sakai, S. et al. Cutting edge: control of *Mycobacterium tuberculosis* infection by a subset of lung parenchyma-homing CD4 T cells. *J. Immunol.* **192**, 2965–2969 (2014).
14. Takagi, T. et al. Heme oxygenase-1 prevents murine intestinal inflammation. *J. Clin. Biochem. Nutr.* **63**, 169–174 (2018).
15. Zhong, H., Bao, W., Friedman, D. & Yazdanbakhsh, K. Hemin controls T cell polarization in sickle cell alloimmunization. *J. Immunol.* **193**, 102–110 (2014).
16. MacMicking, J. D. et al. Identification of nitric oxide synthase as a protective locus against tuberculosis. *Proc. Natl Acad. Sci. USA* **94**, 5243–5248 (1997).
17. Mishra, B. B. et al. Nitric oxide prevents a pathogen-permissive granulocytic inflammation during tuberculosis. *Nat. Microbiol.* **2**, 17072 (2017).
18. Gozzelino, R., Jeney, V. & Soares, M. P. Mechanisms of cell protection by heme oxygenase-1. *Annu. Rev. Pharmacol. Toxicol.* **50**, 323–354 (2010).
19. Singh, N., Ahmad, Z., Baid, N. & Kumar, A. Host heme oxygenase-1: friend or foe in tackling pathogens? *IUBMB Life* **70**, 869–880 (2018).
20. Picard, V., Epsztejn, S., Santambrogio, P., Cabantchik, Z. I. & Beaumont, C. Role of ferritin in the control of the labile iron pool in murine erythroleukemia cells. *J. Biol. Chem.* **273**, 15382–15386 (1998).
21. Soares, M. P. & Bach, F. H. Heme oxygenase-1: from biology to therapeutic potential. *Trends Mol. Med.* **15**, 50–58 (2009).
22. Silva-Gomes, S., Appelberg, R., Larsen, R., Soares, M. P. & Gomes, M. S. Heme catabolism by heme oxygenase-1 confers host resistance to *Mycobacterium tuberculosis* infection. *Infect. Immun.* **81**, 2536–2545 (2013).
23. Kovtunovych, G., Eckhaus, M. A., Ghosh, M. C., Ollivierre-Wilson, H. & Rouault, T. A. Dysfunction of the heme recycling system in heme oxygenase 1-deficient mice: effects on macrophage viability and tissue iron distribution. *Blood* **116**, 6054–6062 (2010).
24. Abdalla, M. Y., Ahmad, I. M., Switzer, B. & Britigan, B. E. Induction of heme oxygenase-1 contributes to survival of *Mycobacterium abscessus* in human macrophages-like THP-1 cells. *Redox Biol.* **4**, 328–339 (2015).
25. Paez, A. V. et al. Heme oxygenase-1 in the forefront of a multi-molecular network that governs cell-cell contacts and filopodia-induced zippering in prostate cancer. *Cell Death Dis.* **7**, e2570 (2016).
26. Pek, R. H. et al. Hemozoin produced by mammals confers heme tolerance. *eLife* **8**, e49503 (2019).
27. Soares, M. P. & Hamza, I. Macrophages and iron metabolism. *Immunity* **44**, 492–504 (2016).
28. Chinta, K. C. et al. Microanatomic distribution of myeloid heme oxygenase-1 protects against free radical-mediated immunopathology in human tuberculosis. *Cell Rep.* **25**, 1938–1952 e1935 (2018).
29. Luz, N. F. et al. *Lutzomyia longipalpis* saliva induces heme oxygenase-1 expression at bite sites. *Front. Immunol.* **9**, 2779 (2018).
30. Singh, N. et al. Antimycobacterial effect of IFN $\gamma$  (interferon gamma)-induced autophagy depends on HMOX1 (heme oxygenase 1)-mediated increase in intracellular calcium levels and modulation of PPP3/calcineurin-TFEB (transcription factor EB) axis. *Autophagy* **14**, 972–991 (2018).



31. Jansen, T. & Daiber, A. Direct antioxidant properties of bilirubin and biliverdin. Is there a role for biliverdin reductase? *Front. Pharmacol.* **3**, 30 (2012).
32. Otterbein, L. E. et al. Carbon monoxide has anti-inflammatory effects involving the mitogen-activated protein kinase pathway. *Nat. Med.* **6**, 422–428 (2000).
33. Lin, J. Y., Seguin, R., Keller, K. & Chadee, K. Tumor necrosis factor alpha augments nitric oxide-dependent macrophage cytotoxicity against *Entamoeba histolytica* by enhanced expression of the nitric oxide synthase gene. *Infect. Immun.* **62**, 1534–1541 (1994).
34. Duvigneau, J. C. et al. A novel endotoxin-induced pathway: upregulation of heme oxygenase 1, accumulation of free iron, and free iron-mediated mitochondrial dysfunction. *Lab. Invest.* **88**, 70–77 (2008).
35. Wang, Q. M. et al. Inhibiting heme oxygenase-1 attenuates rat liver fibrosis by removing iron accumulation. *World J. Gastroenterol.* **19**, 2921–2934 (2013).
36. Weiss, G. et al. Iron regulates nitric oxide synthase activity by controlling nuclear transcription. *J. Exp. Med.* **180**, 969–976 (1994).
37. Boelaert, J. R., Vandecasteele, S. J., Appelberg, R. & Gordeuk, V. R. The effect of the host's iron status on tuberculosis. *J. Infect. Dis.* **195**, 1745–1753 (2007).
38. Harrington-Kandt, R. et al. Hepcidin deficiency and iron deficiency do not alter tuberculosis susceptibility in a murine *M.tb* infection model. *PLoS ONE* **13**, e0191038 (2018).
39. Amaral, E. P. et al. A major role for ferroptosis in *Mycobacterium tuberculosis*-induced cell death and tissue necrosis. *J. Exp. Med.* **216**, 556–570 (2019).
40. Komarov, A. M., Mattson, D. L., Mak, I. T. & Weglicki, W. B. Iron attenuates nitric oxide level and iNOS expression in endotoxin-treated mice. *FEBS Lett.* **424**, 253–256 (1998).
41. Agoro, R., Taleb, M., Quesniaux, V. F. J. & Mura, C. Cell iron status influences macrophage polarization. *PLoS ONE* **13**, e0196921 (2018).
42. Dlaska, M. & Weiss, G. Central role of transcription factor NF-IL6 for cytokine and iron-mediated regulation of murine inducible nitric oxide synthase expression. *J. Immunol.* **162**, 6171–6177 (1999).
43. Hartmann, H. et al. Hypoxia-independent activation of HIF-1 by enterobacteriaceae and their siderophores. *Gastroenterology* **134**, 756–767 (2008).
44. Phelan, J. J. et al. Modulating iron for metabolic support of TB host defense. *Front. Immunol.* **9**, 2296 (2018).
45. Riboldi, E. et al. Hypoxia-mediated regulation of macrophage functions in pathophysiology. *Int. Immunol.* **25**, 67–75 (2013).
46. Fritsche, G., Nairz, M., Werner, E. R., Barton, H. C. & Weiss, G. Nramp1-functionality increases iNOS expression via repression of IL-10 formation. *Eur. J. Immunol.* **38**, 3060–3067 (2008).
47. Drummond, G. S. & Kappas, A. Prevention of neonatal hyperbilirubinemia by tin protoporphyrin IX, a potent competitive inhibitor of heme oxidation. *Proc. Natl Acad. Sci. USA* **78**, 6466–6470 (1981).
48. Kappas, A., Drummond, G. S., Manola, T., Petmezaki, S. & Valaes, T. Sn-protoporphyrin use in the management of hyperbilirubinemia in term newborns with direct Coombs-positive ABO incompatibility. *Pediatrics* **81**, 485–497 (1988).
49. Dover, S. B., Graham, A., Fitzsimons, E., Moore, M. R. & McColl, K. E. Haem-arginate plus tin-protoporphyrin for acute hepatic porphyria. *Lancet* **338**, 263 (1991).
50. Dover, S. B., Moore, M. R., Fitzsimons, E. J., Graham, A. & McColl, K. E. Tin protoporphyrin prolongs the biochemical remission produced by heme arginate in acute hepatic porphyria. *Gastroenterology* **105**, 500–506 (1993).
51. Schulz, S., Wong, R. J., Vreman, H. J. & Stevenson, D. K. Metalloporphyrins—an update. *Front. Pharmacol.* **3**, 68 (2012).
52. Berglund, L. et al. Heme oxygenase inhibitors transiently increase serum ferritin concentrations without altering other acute-phase reactants in man. *Pharmacology* **59**, 51–56 (1999).
53. Kappas, A., Drummond, G. S. & Galbraith, R. A. Prolonged clinical use of a heme oxygenase inhibitor: hematological evidence for an inducible but reversible iron-deficiency state. *Pediatrics* **91**, 537–539 (1993).
54. Pittala, V., Salerno, L., Romeo, G., Modica, M. N. & Siracusa, M. A. A focus on heme oxygenase-1 (HO-1) inhibitors. *Curr. Med. Chem.* **20**, 3711–3732 (2013).
55. Cardona, P. J. The progress of therapeutic vaccination with regard to tuberculosis. *Front. Microbiol.* **7**, 1536 (2016).
56. Groschel, M. I., Prabowo, S. A., Cardona, P. J., Stanford, J. L. & van der Werf, T. S. Therapeutic vaccines for tuberculosis—a systematic review. *Vaccine* **32**, 3162–3168 (2014).
57. Cosma, C. L., Humbert, O. & Ramakrishnan, L. Superinfecting mycobacteria home to established tuberculous granulomas. *Nat. Immunol.* **5**, 828–835 (2004).
58. Philippot, Q. et al. Increased iron sequestration in alveolar macrophages in chronic obstructive pulmonary disease. *PLoS ONE* **9**, e96285 (2014).
59. Schneider, C. A., Rasband, W. S. & Eliceiri, K. W. NIH Image to ImageJ: 25 years of image analysis. *Nat. Methods* **9**, 671–675 (2012).